Optimization of the leak conductance in the squid giant axon

Jeffrey Seely and Patrick Crotty*
Department of Physics and Astronomy, Colgate University, 13 Oak Drive, Hamilton, New York 13346, USA
(Received 19 May 2009; revised manuscript received 14 May 2010; published 6 August 2010)

We report on a theoretical study showing that the leak conductance density, G_L, in the squid giant axon appears to be optimal for the action potential firing frequency. More precisely, the standard assumption that the leak current is composed of chloride ions leads to the result that the experimental value for G_L is very close to the optimal value in the Hodgkin-Huxley model, which minimizes the absolute refractory period of the action potential, thereby maximizing the maximum firing frequency under stimulation by sharp, brief input current spikes to one end of the axon. The measured value of G_L also appears to be close to optimal for the frequency of repetitive firing caused by a constant current input to one end of the axon, especially when temperature variations are taken into account. If, by contrast, the leak current is assumed to be composed of separate voltage-independent sodium and potassium currents, then these optimizations are not observed.

DOI: 10.1103/PhysRevE.82.021906 PACS number(s): 87.19.lb, 87.19.ll, 87.19.lo, 02.60.Pn

I. INTRODUCTION

A considerable amount of evidence has emerged in recent years to show that many of the parameters which govern the structure and function of biological nervous systems are at optimal values for metabolic energy consumption, information rates, or some combination thereof, presumably because of evolutionary pressures [1–3]. Many of these studies have focused on the squid giant axon because of its well-known and relatively simple properties. Hodgkin and Adrian hypothesized as early as the 1970s that the channel densities in the squid giant axon are at values that maximize the action potential velocity [4,5], although more updated axon models have called this into question [6] and suggested that axons are optimized for the energy associated with the action potential instead [7,8]. There are a large number of independently variable parameters that significantly affect the functioning of the squid giant axon, only a few of which have been systematically investigated for possible optimizations. Here, we present results for one of them: the leak conductance.

The voltage-independent leak conductance is one of three conductances known to be present in the squid giant axon. With a measured value of about 0.3 $\mathrm{mS/cm^2}$, it is much smaller in magnitude than the maximum voltage-gated Na^+ (120 $\mathrm{mS/cm^2}$) and K^+ (36 $\mathrm{mS/cm^2}$) conductances, yet it nevertheless plays an important role in the electrical stability of the axon. Leak conductances are known to be present in many other kinds of neurons as well, such as molluscan pacemaker cells [9].

Because of its small size, there has long been debate about the exact nature of the leak conductance, with some of the debate centering on how much of it is due to voltage-gated K^+ and Na^+ channels that remain open at rest [10,11]. However, a nonselective, voltage-independent cation channel protein has recently been conclusively identified in mammalian neurons [12]. In squid giant axons, the closeness of the leak reversal potential to the equilibrium potential of Cl^- has traditionally been taken to indicate that chloride ions are a significant contributor to the current, although there may be others [13].

Given the possibility that the leak conductance is an easily evolvable parameter capable of influencing the electrical properties of axons, it is natural to ask whether the leak conductance is at an optimal value for some quantity related to information processing or energy consumption. Here, we present results showing that the leak conductance is near optimal for the absolute and repetitive firing frequency of the axon if the leak current is assumed to be chloride, but not if it is sodium/potassium. For completeness we also investigated the effects of G_L on the relative refractory period, which is substantially harder to calculate numerically. We did not find strong evidence that G_L is optimal in this case for either channel model.

II. METHODS

A. Hodgkin-Huxley model

The squid giant axon, about 0.5 mm in diameter, is one of the largest axons in nature. It innervates muscles in the squid mantle, and its action potentials cause the muscles to contract, expelling a brief jet of water and allowing the squid to move away quickly from danger. The axon is postsynaptic to neurons in the dorsal magnocellular lobe, and it is indirectly connected to the ventral magnocellular lobe, which integrates sensory input.

Fortunately, the squid giant axon is also one of the simplest known axons, being unmyelinated and having only two voltage-gated ion channels with relatively straightforward kinetics. As such, we arguably know more about the squid giant axon than any other neural system, and it is possible to model it to a high degree of biological accuracy. The Hodgkin-Huxley (HH) model, based on the experiments of A. L. Hodgkin and A. F. Huxley in 1952 [14], remains very useful, although subsequent refinements to the sodium and potassium channel kinetics have been made [15,16]. In our study, we used the traditional version of the HH model described below.

*Corresponding author; pcrotty@colgate.edu

The model treats the squid giant axon as a cylinder of length L and uniform diameter d. For most of our simulations, L was set to 0.8 cm. The diameter was generally in the range of 300–600 μm. (These dimensions are typical of the biological ones.) The cylinder has an axial resistivity R_a representing the axoplasm. This was generally set to 35.4 $\Omega\cdot$cm after Hodgkin and Huxley's measurement. Transmembrane currents flow through two voltage-dependent Na^+ and K^+ conductances, G_{Na} and G_K, and a voltage-independent leak conductance, G_L. The Hodgkin-Huxley experimental measurements of G_L ranged from 0.13 to 0.5 mS/cm^2, with an average of about 0.26 mS/cm^2 [13]. It was primarily this value that we varied in our simulations. The voltage-dependent conductances are functions of time and, indirectly, the membrane potential:

$$G_{Na} = \bar{G}_{Na}[m(t)]^3 h(t), \tag{1}$$

$$G_K = \bar{G}_K[n(t)]^4, \tag{2}$$

where m and h are state variables representing the fraction of Na^+ channel subunits in the open and non-inactivated states, respectively, and n is the state variable representing the fraction of open K^+ channel subunits (squid K^+ channels do not inactivate). Each of the four subunits in a channel has to be open or noninactivated in order for the channel to pass ions. Thus, m^3h and n^4 are, respectively, the fraction of Na^+ and K^+ channels which are open. These state variables evolve according to Eq. (4) below. The maximal conductances, $\bar{G}_{Na}$ and $\bar{G}_K$, obtain when all the channels are open. We used Hodgkin and Huxley's experimental values of $\bar{G}_{Na}=120$ mS/cm^2 and $\bar{G}_K=36$ mS/cm^2.

The cell membrane has a constant intrinsic capacitance of approximately $C_0=0.88$ μF/cm^2 [17]. The voltage-gated sodium channels also contribute a phenomenological capacitance, $C_g=0.13$ μF/cm^2, the so-called "gating" capacitance [5]. (In principle, the voltage-gated potassium channels contribute a gating capacitance too, but this is so much smaller than the sodium gating capacitance that it can be neglected.)

Electrical excitations of the axon are described by four coupled differential equations. The first of these is a modified version of the cable equation:

$$\frac{d}{4R_a}\frac{d^2V}{dx^2} = (C_0 + C_g)\frac{dV}{dt} + \bar{G}_{Na}m^3h(V - E_{Na}) + \bar{G}_K n^4(V - E_K) + G_L(V - E_L), \tag{3}$$

where V is the cross-membrane potential, with the extracellular side taken as ground. The Na^+ and K^+ reversal potentials, E_{Na} and E_K, are determined by the ionic concentration gradients across the membrane: the values we used, $E_{Na}=50$ mV and $E_K=-77$ mV, are typical of the squid giant axon. The leak reversal potential, E_L, is determined by the ion(s) which pass through the leak channels and is experimentally around −55 mV [13]. We discuss our leak channel assumptions in greater detail below.

The other three differential equations govern the gating variables:

$$\frac{ds}{dt} = \alpha_s(V)(1 - s) - \beta_s(V)s, \tag{4}$$

where $s=n$, m, or h. The rate coefficients, α_s and β_s, are the fraction of s subunits per unit time switching from closed/inactivated to open and open to closed/inactivated, respectively. These rates were empirically measured by Hodgkin and Huxley as:

$$\alpha_m(V) = \phi \times 0.1\frac{-(V+40)}{(e^{-(V+40)/10} - 1)} \ [\text{ms}^{-1}] \tag{5}$$

$$\beta_m(V) = \phi \times 0.4e^{-(V+65)/18} \ [\text{ms}^{-1}] \tag{6}$$

$$\alpha_h(V) = \phi \times 0.07e^{-(V+65)/20} \ [\text{ms}^{-1}] \tag{7}$$

$$\beta_h(V) = \phi \times \frac{1}{(e^{-(V+35)/10} + 1)} \ [\text{ms}^{-1}] \tag{8}$$

$$\alpha_n(V) = \phi \times 0.01\frac{-(V+55)}{(e^{-(V+55)/10} - 1)} \ [\text{ms}^{-1}] \tag{9}$$

$$\beta_n(V) = \phi \times 0.125e^{-(V+65)/80} \ [\text{ms}^{-1}] \tag{10}$$

with V in mV. The temperature coefficient ϕ is

$$\phi = 3^{(T-6.3)/10} \tag{11}$$

with T in °C. It should be noted that the openings and closings of individual ion channels are stochastic in nature; Eq. (4) describes the average behavior of a large ensemble of s-subunits.

Equations (3) and (4) are highly nonlinear [Eq. (4) because of the forms of the rate coefficients Eqs. (5)–(10)]; and, without significant approximations, they are analytically intractable. However, it is known that they have a unique solution describing a single voltage spike, or "action potential," propagating at a uniform velocity v_{AP} along the axon. The action potential velocity is a function of the different biophysical parameters in Eqs. (3)–(10), though it does not have an exact analytical form and must generally be either approximated or determined numerically.

Our simulated axon contained 1000 isopotential segments, each of length 100 μm. Equations (3) and (4) (for n, m, and h) were solved simultaneously in each segment using an implicit backward Euler method. Our time step was 1 μs. We verified that the time and spatial resolutions were sufficiently fine so as to not significantly influence our results. We assumed $T=18.5$ °C unless stated otherwise.

B. Leak channel

We tested two different assumptions about the nature of the leak channel. We assumed first that it is a voltage-independent Cl^- conductance, in which case the leak reversal potential, E_L, is just the equilibrium potential of chloride:

$$E_L = E_{Cl} \approx -55 \ \text{mV}. \tag{12}$$

We identify this case as "Cl^- leak" in the figures. In our simulations, we typically varied the value of G_L while keep-

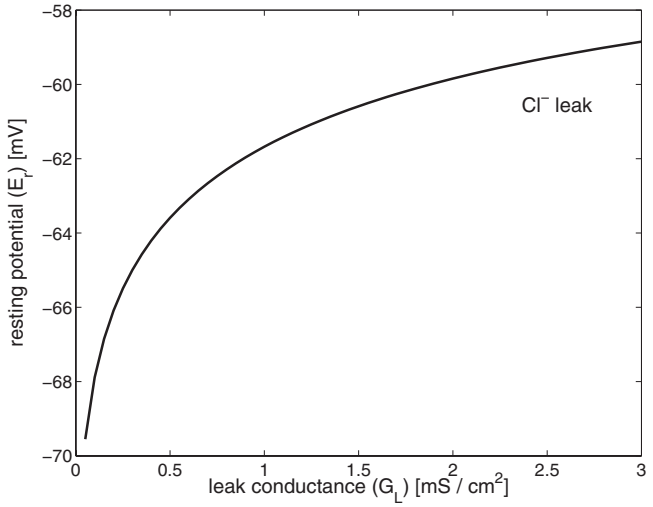

FIG. 1. Despite its small magnitude, G_L has a significant effect on the resting potential of the axon, E_r, defined as the potential at which there is no net transmembrane current. Here we plot E_r as a function of G_L while keeping all other parameters fixed (this therefore corresponds to the case of Cl^- leak channels.)

ing all the other parameter values the same. This has the effect of changing the resting potential of the axon (see Fig. 1) and, indirectly, the maximum frequency at which action potentials can fire. We numerically calculated the new resting potential and set the axon to this value at the beginning of our simulations before action potentials were evoked.

In the second case, we assumed that the leak channel consists of two voltage-independent Na^+ and K^+ conductances, in which case E_L is determined by a weighted average of E_{Na} and E_K:

$$E_L = \frac{G_{LK}E_K + G_{LNa}E_{Na}}{G_{LK} + G_{LNa}}. \tag{13}$$

In this case, which is identified as "Na^+/K^+ leak" in the figures, the total leak conductance is just the sum of the sodium and potassium leak conductances:

$$G_L = G_{LNa} + G_{LK}. \tag{14}$$

Since only G_L and E_L appear in the equation of motion for V, Eq. (3), the refractory periods are not affected by whether it is Cl^- or Na^+/K^+ that goes through the leak channel if only G_L is varied. That is, any optimization results involving the leak conductance alone that obtain for Cl^- leak channels should obtain for Na^+/K^+ leak channels as well—or, in fact, for a leak current composed of any combination of permanent ions, provided that their overall reversal potential is approximately E_{Cl}. In order to more completely distinguish between the two cases, we added the further requirement in the Na^+/K^+ leak channel case that whenever the value of G_L was altered, the value of E_L was altered as well so as to keep the overall resting potential, E_r, at −65 mV. This is equivalent to altering the ratio of the Na^+ leak conductance, G_{LNa}, to the K^+ leak conductance, G_{LK}, while keeping the reversal potentials E_{Na} and E_K the same.

Thus, the mathematical distinction between the two models is that for Cl^- leak channels, only G_L is varied in Eq. (3), which in turn causes the resting potential to vary as shown in Fig. 1. For Na^+/K^+ channels, by contrast, both G_L and E_L are varied in tandem so as to keep the resting potential at −65 mV.

The next generalization of these models would be to allow both G_L and E_L to vary independently, which would also change E_r to varying degrees: for example, if G_L were very large, E_r would be pulled toward E_L, while if G_L were very small, the value of E_L would have little effect on E_r. Systematic investigations of the optimizations discussed here in such an extended model would be challenging due to the high computational costs of multidimensional parameter sweeps.

C. Simulations

All of our simulations were done using the NEURON/NMODL neuronal modeling language [18] and auxiliary parameter-sweeping codes written in C and Python. We systematically varied G_L in Eq. (3) and occasionally other parameters, which are described in further detail in Sec. III, in order to determine how they influence the absolute and relative refractory periods of the action potential and the frequency of repetitive firing.

Simulated action potentials were evoked in two different ways. When studying the absolute and relative refractory periods, action potentials were evoked by 1 A, 1 μs duration current injections into one end of the axon; we verified that these values were sufficiently brief and large so as to not influence the refractory periods. They are referred to throughout the text as "current spike-evoked" action potentials. The absolute refractory period, T_{abs}, was determined by finding the maximum time between successive current injections such that only one action potential resulted. We verified that for inter-injection times just above the absolute refractory period, two action potentials were produced and both propagated down the full length of the axon, as expected. The maximum possible action potential firing frequency, i.e., the maximum frequency at which the axon can be driven with current spike inputs, is then the reciprocal of the absolute refractory period, f_{max}:

$$f_{max} = \frac{1}{T_{abs}}. \tag{15}$$

If the time interval between the input current spikes is greater than T_{abs} but less than a certain value T_{rel}, called the relative refractory period, then while a second action potential is generated, it is generated in the wake of the first one, when the membrane and the voltage-gated ion channels have not yet returned to their resting states. The result is that the two action potentials interfere with each other: the velocity of the second is different from that of the first, and the distance between the action potentials—or, equivalently, the time between their peaks as measured at a single point along the axon—changes as they move down the axon. Information encoded in the distribution of intervals between action potentials can therefore be corrupted if they are too close to-

gether. If T_i is the time between the two current spikes and T_{AP} is the time between the peaks of the two resulting action potentials as measured at some point further down the axon, then we can define the "interval shift" as $\Delta T \equiv T_{AP} - T_i$. For $T_i \geq T_{rel}$, $T_{AP} = T_i$ and so $\Delta T = 0$.

It is somewhat difficult to determine T_{rel} numerically. Action potentials in the Hodgkin-Huxely model have a phase of small, damped oscillations around the resting potential after the peak, which means that a second closely following action potential can be either sped up or slowed down depending on which part of an oscillation it falls into. As a result, the interval shift ΔT itself oscillates around 0 as a function of T_i (Fig. 9 and [19]), and this causes T_{rel} as a function of G_L to have a jagged, discontinuous appearance (Fig. 8). Moreover, jitter noise in biological axons (caused by phenomena such as ion channel flicker) puts a nonzero lower bound on the timing resolution of consecutive action potentials.

Thus, it is both computationally easier and probably more biologically relevant to define a relative refractory period as a function of the maximum interval shift: for all values of T_i greater than $T_{rel}(\Delta T_{max})$, by definition, $|\Delta T| = |T_{AP} - T_i| \leq \Delta T_{max}$, where $\Delta T_{max} > 0$. The reciprocal of $T_{rel}(\Delta T_{max})$ gives the maximum frequency, $f_{rel}(\Delta T_{max})$, at which the axon can be driven with an interval shift no larger than ΔT_{max}:

$$f_{rel}(\Delta T_{max}) = \frac{1}{T_{rel}(\Delta T_{max})}. \tag{16}$$

We determined $T_{rel}(\Delta T_{max})$ for values of ΔT_{max} ranging from 1 μs (the numerical resolution of our simulations) up to 1 ms.

To determine the repetitive firing frequency, f_r, we simulated a constant (time-independent) current input, I_{DC}, to one end of the axon. We then tested whether regular, repetitive firing resulted and, if so, measured the time between equivalent points on successive action potentials 20 ms after the beginning of the input current, by which time any initial transients had long since disappeared. The reciprocal of this time was then f_r, which in general depended on the value of I_{DC} as well as that of G_L. We refer to f_r as the "repetitive firing frequency."

We generally measured the time intervals between successive action potentials at a point 8 cm down the axon from the input stimuli. We verified that our optimization results were insensitive to the actual location of this point as long as it was outside a small region near the current injection site.

III. RESULTS

A. Resting potential and individual action potentials

In addition to the effects of G_L on firing frequencies, which is the main focus of this study, G_L also affects the shapes of individual action potentials and, in the case of Cl^- channels, the overall resting potential of the axon. The resting potential E_r is the voltage at which the sum of all the steady-state ionic currents is 0 (Fig. 1). It is therefore determined by the leak current as well as the small currents through the voltage-gated sodium and potassium channels, which are almost (but not entirely) closed at E_r. Physically, the resting potential is determined by the channel densities, the ionic concentration gradients, and the steady-state conformational configurations of the voltage-gated channels.

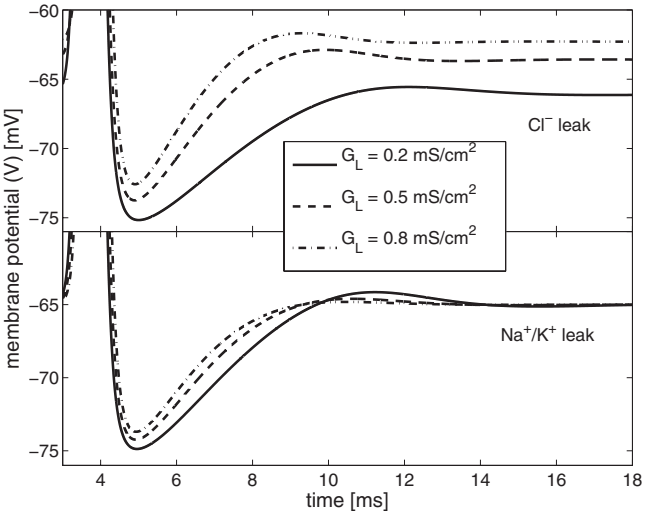

FIG. 2. At lower values of the leak conductance, the axon takes longer to return to rest after a current spike-evoked action potential. Note that the resting potential is always made to be −65 mV for the Na^+/K^+ case.

Using the standard (and reasonably well established) values of these other parameters, as G_L increases from 0.05 to 3 mS/cm^2, the resting potential increases (in the sense of getting less negative) by roughly 10 mV, with the sharpest rate of increase in the range below 1 mS/cm^2. For Na^+/K^+ channels, there is no such dependence of E_r on G_L because, as discussed above, we simultaneously varied the ratio of Na^+ and K^+ leak conductances in order to keep E_r at −65 mV.

The effects of G_L on individual (current spike-evoked) action potentials differ between the two models. With Cl^- channels, higher values of G_L lead to smaller and narrower spikes that have a more pronounced postpeak oscillation. With Na^+/K^+ channels, by contrast, the heights and widths of the main action potential peaks are not significantly affected by G_L. In both models, smaller values of G_L cause the membrane potential to take longer to return to E_r after an action potential (Fig. 2); however, the postpeak oscillations are larger for larger G_L in the Cl^- model, while they are smaller for larger G_L in the Na^+/K^+ model.

We also investigated the effects of G_L on the metabolic energy consumption associated with action potentials, in view of other work [7,8] suggesting that the overall scale of the three conductances in the squid giant axon is optimized for the energy associated with action potential velocity. We did not find any such optimizations for G_L alone, but only a monotonic increase in metabolic energy consumption with increasing G_L.

B. Maximum firing frequency

Figures 3 and 4 show some of our central results, the maximum firing frequency, f_{max}, calculated as a function of G_L. In the Cl^- model, for values of G_L much above the ex-

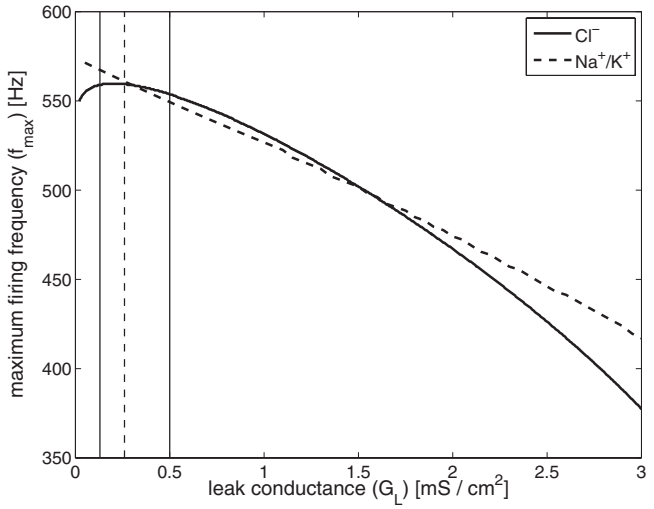

FIG. 3. For Cl^- leak channels, the maximum firing frequency has a maximum value of about 560 Hz when G_L is around 0.2 mS/cm^2, in the range of experimentally measured values. By contrast, there is no local maximum for Na^+/K^+ leak channels: f_{max} increases monotonically with decreasing G_L. Here and in subsequent figures, the two solid vertical lines show the range of G_L measured by Hodgkin and Huxley, while the dashed vertical line shows the mean value of their measurements. The G_L resolution in all simulations is 0.005 mS/cm^2.

perimental range, f_{max} decreases by about 80 Hz for each 1 mS/cm^2 increase in G_L (although the rate of decrease is slightly superlinear).

However, as is just barely visible in Fig. 3 and much more evident in Fig. 4, the relationship between f_{max} and G_L in the Cl^- model is not monotonic. For very low values of G_L, f_{max} instead increases with G_L, attaining a maximum value of about 560 Hz at 18.5 °C near $G_L=0.2$ mS/cm^2. Within the numerical limits of our simulation, the f_{max}-optimal value of G_L for the Cl^- model is about 0.2 ± 0.06 mS/cm^2, well

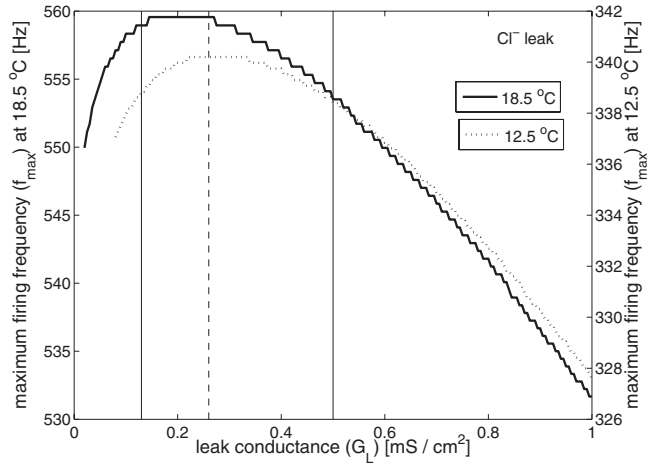

FIG. 4. The region around the Cl^- leak model f_{max} maximum in Fig. 3 is shown in greater resolution at two different temperatures. The 18.5 °C case has its maximum at $G_L\approx0.2\pm0.06$. At 12.5 °C, the maximum f_{max} is at $G_L\approx0.27\pm0.06$ and has a value of about 340 Hz. The jagged shape of the curve and flatness near the minimum are due to the numerical limits of the simulation.

within the range of experimentally measured values.

In the Na^+/K^+ model, however, f_{max} decreases monotonically by about 60 Hz for every 1 mS/cm^2 increase in G_L. This may be due to the different way G_L affects the action potentials in this case (Fig. 2). The optimal value of G_L in this model for maximum firing frequency is therefore 0.

Since the rate coefficients [Eqs. (5)–(10)] have a strong dependence on temperature, we repeated our calculations at 12.5 °C and 25 °C, representative of the range of temperatures the *Loligo* squid genus studied by Hodgkin and Huxley would normally experience. At both of these temperatures and for both of the models, we found qualitatively similar behavior as at 18.5 °C. In the Cl^- model, the maximum values of f_{max} occur in or near the experimental range of G_L (although the value of the maximum f_{max} itself increases substantially with temperature, from about 340 Hz at 12.5 °C to 848 Hz at 25 °C). The optimal value of G_L decreases with increasing temperature from $G_L\approx0.27$ mS/cm^2 at 12.5 °C (Fig. 4) to $G_L\approx0.11$ mS/cm^2 at 25 °C. In both cases, the area around the maximum is fairly flat (although slightly less so for the 25 °C case) with a width of about 0.06 mS/cm^2. While the optimal G_L is therefore not temperature-independent, the relative flatness of the maxima means that the maximum firing frequency for values of G_L near, for example, 0.2 mS/cm^2 are either at the maximum or within 2–3 Hz of it.

In the Na^+/K^+ case, the relationship between G_L and f_{max} at the other temperatures is still monotonically decreasing with no local maximum. Additionally, no local maxima were observed when the magnitudes of the active sodium and potassium conductances, rather than the leak conductance, were varied.

C. Repetitive firing frequency

It is known [20] from both theory and experiment that a constant current input to one end of a non-space-clamped axon can produce repetitive firing at a constant frequency, albeit only over a fairly narrow range of current. We investigated how the value of G_L affects this firing frequency, f_r, which is qualitatively different than the firing produced by current spikes discussed above.

For the Na^+/K^+ channel model, as with the maximum firing frequency, we found no evidence of an optimization of G_L at nonzero values for f_r. The picture is considerably more complex, however, for the Cl^- model. Over a fairly large range of input current and temperature, f_r attains its maximum value in or near the experimental range of G_L. In Fig. 5, we show f_r versus G_L for both models at typical values of temperature and input current. The Cl^- f_r maximum in this case is about 208 Hz at $G_L=0.265$ mS/cm^2.

However, the value of I_{DC} is a second independent parameter (assuming we hold all others fixed), and thus, in contrast to the maximum firing frequency produced by discrete current spikes (which is independent of their actual size), we must analyze the repetitive firing frequency as a function of both the leak conductance and the constant input current. In Fig. 6, we show the repetitive firing frequency in the two-dimensional G_L-I_{DC} parameter space. The bold curve shows

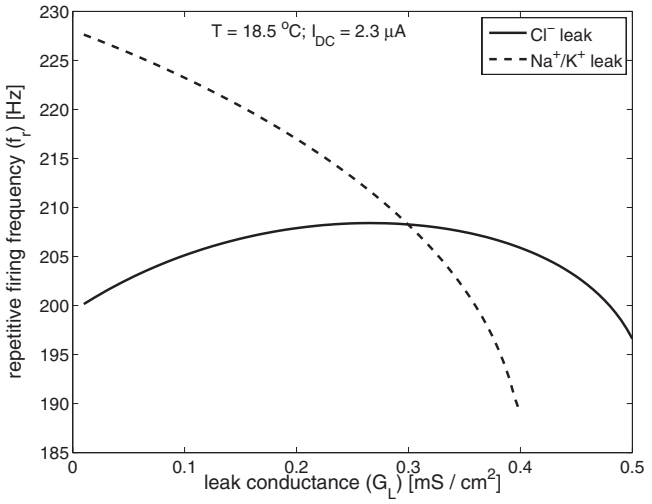

FIG. 5. The repetitive firing frequency, f_r, i.e., the action potential frequency caused by a constant current input (I_{DC}) of 2.3 μA at one end of the axon, is shown as a function of G_L. As before, no local maximum is evident for the Na^+/K^+ leak channel model, and for it f_r increases with decreasing G_L. However, the Cl^- model once again attains a maximum well above vanishing G_L. For this value of I_{DC} and over a fairly large range in general, the maximum is very near the experimental value of G_L.

the limits of the region where repetitive firing can occur. For combinations of G_L and I_{DC} outside it, repetitive firing either does not occur or lasts for only a few spikes. The dashed curve within shows the f_r-optimal value of G_L as a function of I_{DC}; e.g., at I_{DC}=2.5 μA, the maximum f_r of 218 Hz occurs when G_L is about 0.255 mS/cm^2. If G_L is larger or

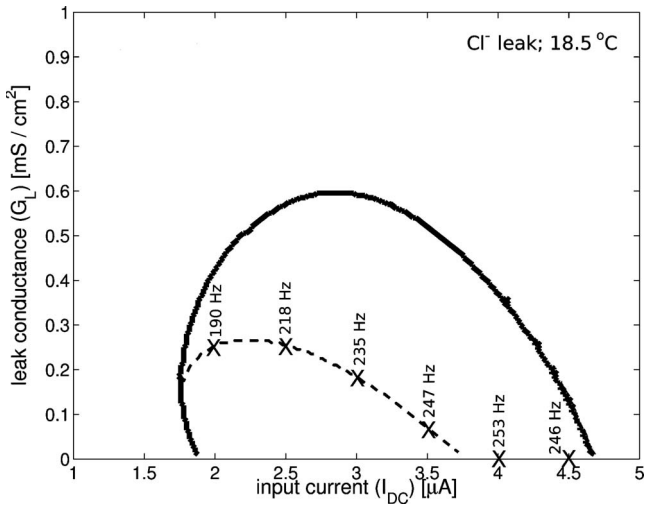

FIG. 6. We show the behavior of the repetitive firing frequency in two-dimensional (G_L-I_{DC}) parameter space. The solid black curve shows the boundary of the region outside which a constant input current to one end of the axon does not produce sustained repetitive firing. The dashed curve inside the boundary shows the optimal value of G_L for f_r as a function of I_{DC}. The numbers along the curve show the actual value of f_r at various points. For the upper third of the I_{DC} range inside the boundary, the highest value of f_r is attained when G_L vanishes; for most of the rest, however, the optimal G_L is in the experimental range.

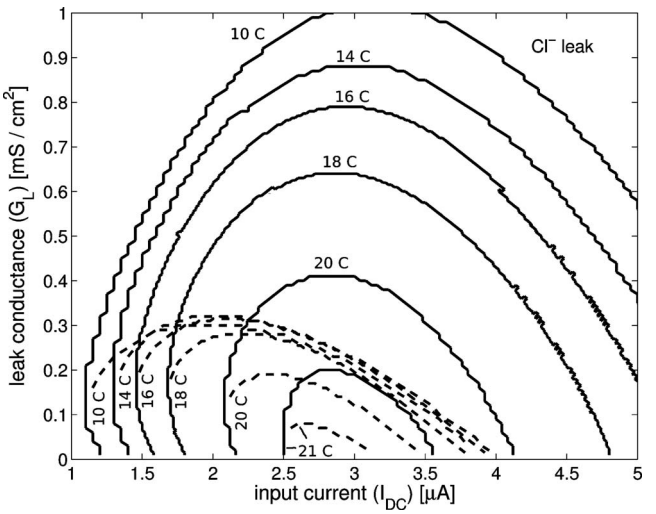

FIG. 7. We show the same information as in Fig. 6 but for a range of temperature characteristic of what squid in the ocean encounter over periods of a few months. In general, higher temperatures decrease the size of the region of parameter space in which repetitive firing occurs. The optimal G_L value for a given I_{DC} is relatively temperature-independent except at high temperatures or low I_{DC} values.

smaller than this, f_r decreases in a way similar to what is shown in Fig. 5.

One evident feature of Fig. 6 is that no repetitive firing at all is possible for values of G_L above about 0.6 mS/cm^2, regardless of the value of I_{DC}. This maximum upper limit of G_L depends on temperature, as we will discuss, but is always below about 1 mS/cm^2 for temperatures above about 10 °C. Thus, G_L must be much smaller than the maximum voltage-gated sodium and potassium conductances in order for repetitive firing to occur.

Another feature is that over about the lower half of the range of I_{DC} where repetitive firing is possible, the optimal G_L is within the experimental range (0.13 to 0.5 mS/cm^2), and is everywhere below 0.27 mS/cm^2. However, for values of I_{DC} above about 3.8 μA, the maximum f_r obtains when G_L is 0. This includes the overall maximum f_r, 253 Hz, located at I_{DC}=4.08 μA. This value of f_r is several tens of Hz above the maximum f_r values at lower ranges where the optimal G_L is in the experimental range.

In Fig. 7, we show the combined results for an approximately 10 °C range of temperature characteristic of what ocean-dwelling squid encounter over the course of a few months [21]. At warmer temperatures, the range of G_L-I_{DC} parameter space over which repetitive firing is possible decreases sharply. Conversely, the f_r-optimal G_L value as a function of I_{DC} is relatively independent of temperature below the highest temperatures or above the lowest I_{DC} values. Above about 4 μA, the optimal G_L is 0, with the highest absolute f_r value also generally in this range, while for most of the range below, G_L is within the experimental limits.

D. Relative refractory period

As discussed above, the relative refractory period is more easily and probably more relevantly calculated with respect

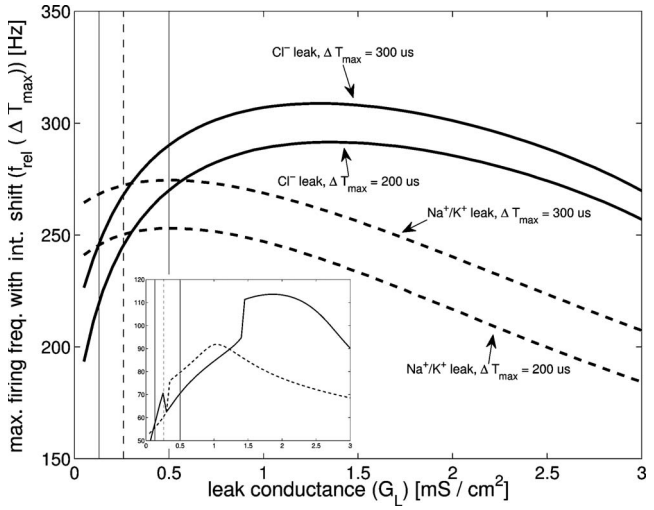

FIG. 8. The maximum firing frequency for a maximum allowed interval shift ΔT_{max} [defined in Eq. (16)] is shown for the two leak channel models for $\Delta T_{max}=200$ and 300 μs. For Cl^- channels, the frequency-optimal G_L is in the range of 1.2–1.3 mS/cm^2, well above the experimental range. For Na^+ and K^+ channels, the optimal G_L is lower but still at the upper end of the experimental range. *Inset*: we show the frequencies for $\Delta T_{max}=2$ μs. At this as well as at other low values of the maximum interval shift, the frequency-optimal G_L values are well outside the experimental range in both the Cl^- (solid) and Na^+/K^+ (dashed) models.

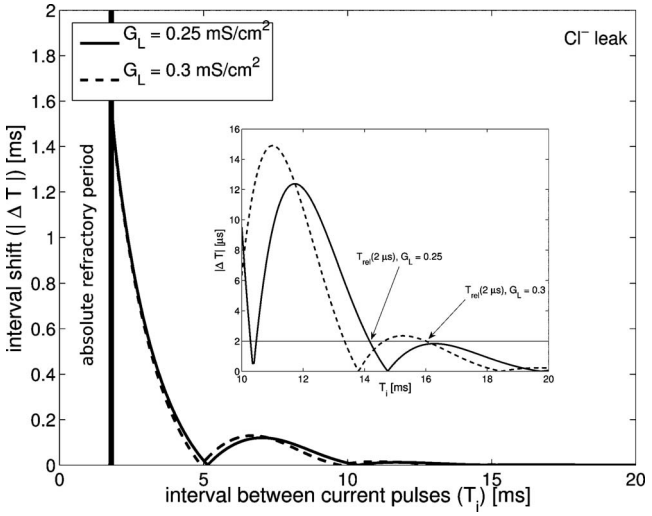

FIG. 9. The absolute value of the interval shift, $|\Delta T|=|T_{AP}-T_i|$, is shown as a function of T_i for two nearby values of G_L. The secondary peaks after $T_i=5$ ms are due to the postpeak oscillations of the first action potential, which can either speed up or slow down the second action potential. Inset: magnified view of the 10 ms $\leq T_i \leq 20$ ms region. The horizontal line shows $|\Delta T|=\Delta T_{max}=2$ μs; the largest T_i value at which it intersects each curve gives $T_{rel}(\Delta T_{max})$.

to a nonzero maximum interval shift ΔT_{max}. In Fig. 8, we show the corresponding maximum firing frequency, $f_{rel}(\Delta T_{max})$, for a very low ΔT_{max}, 2 μs (inset), and then for two higher values, 200 and 300 μs. The higher-ΔT_{max} curves have optimal G_L values substantially outside the experimental range in the case of Cl^- channels, and only barely inside it for Na^+/K^+ channels. For both models, the values of these optima are insensitive to ΔT_{max} provided it is larger than about 150 μs. The Na^+/K^+ optima also appear to be relatively insensitive to other parameters such as temperature and axial resistivity.

The low-ΔT_{max} curves look substantially different, and the reason for this is illustrated in Fig. 9. The relative refractory period for a given ΔT_{max} is calculated by finding the largest value of the initial interval between current stimuli, T_i, such that $|\Delta T|=\Delta T_{max}$; we then define this T_i value as $T_{rel}(\Delta T_{max})$, which can be visualized as the last point where the horizontal line representing ΔT_{max} intersects the T_i vs. $|\Delta T|$ curve. For values of ΔT_{max} larger than about 150 μs, this point always falls on the first, monotonically decreasing part of the curve below $T_i \approx 5$ ms, resulting in the smooth appearance of the high-ΔT_{max} curves in Fig. 8. For low values of ΔT_{max}, however, the point of intersection falls within the region of secondary peaks due to the membrane potential oscillations after the first action potential. The sizes and locations of the secondary peaks depend on G_L. As a result, it is possible for a peak to be just above ΔT_{max} for one value of G_L and just below it for a second, nearby value of G_L, causing a sharp transition in the value of $T_{rel}(\Delta T_{max})$ as a function of G_L. This is the case in the inset to Fig. 9: for $G_L=0.3$ mS/cm^2, the point of intersection is at about $T_i=16$ ms, while for $G_L=0.25$ mS/cm^2, the size of the peak there is slightly below $\Delta T_{max}=2$ μs and therefore the intersection point jumps down to the previous oscillation, at about $T_i=14.2$ ms. We therefore see a sharp spike at $G_L=0.25$ mS/cm^2 in the inset to Fig. 8 for Cl^-. Similar effects are seen in any curve of $f_{rel}(\Delta T_{max})$ vs. G_L for small values of ΔT_{max}.

IV. DISCUSSION

The two scenarios considered here for the stimulation of action potentials in the squid giant axon, delta functionlike current spike inputs and unchanging constant current inputs, represent idealized extremes of the actual biology. The input current to the squid giant axon originates from postsynaptic glutamate-activated sodium channels at the squid giant synapse [22]. The frequency and duration with which these currents are evoked are ultimately determined by the squid's sensory environment, e.g., whether it perceives any predators to be nearby. Thus, the actual current input to the axon when it is active is neither instantaneous nor constant, but is likely to be a time-varying function determined by the rate of synaptic bombardment and the kinetics of the synapse and postsynaptic sodium channels. Because of the relative dearth of experimental data on the operation of the squid giant axon system *in vivo* [23], it is difficult to accurately model this current. However, it might qualitatively be expected that optimization results which hold for the two theoretical extremes would hold for the true time-dependent input current to the axon as well.

Our results indicate that if the input stimulus to the axon can be regarded as a series of discrete, sharp pulses, and if the leak current is assumed to be chloride, then the maximum firing frequency of the axon is itself maximized for values of leak conductance within the experimental range of values.

For continuous input currents (I_{DC}), the same is generally true for at least half of the range of I_{DC} and almost all the range of temperature over which repetitive firing can occur. However, when one considers the full range of G_L-I_{DC} parameter space, the repetitive firing frequency is maximized overall at high values of I_{DC} and $G_L=0$. This raises the question of why, if the input current is constant (or, at least, has a time scale much longer than the repetitive firing frequency), a vanishing leak conductance and high input current level would not be preferable.

One possible reason is metabolic energy consumption: higher I_{DC} values would be associated with larger currents through the Na^+ channels in the synapse as well as more frequent action potentials in the axon itself. This implies that the metabolic energy cost of driving the axon at a frequency f_r, which can be quantified by the overall flux of Na^+ ions into the membrane (all of which has to be subsequently pumped back out by the ATPase Na^+/K^+ exchanger in order to restore the resting concentration gradient), would be substantially higher at higher I_{DC} and f_r values. Of course, presumably it would not be optimal for f_r itself to be too low. Hence, there may be an optimization involving both firing frequency and metabolic energy which would favor the lower end of the I_{DC} range and the observed values of G_L.

A simpler and perhaps more compelling reason is the requirement that the squid giant axon be able to function over a range of ocean temperature that can span 10 or more degrees Celsius over the course of a few months [21], and several degrees over a single day [24]. An important consideration is that both G_L, which depends on the leak channel density on the axon, and I_{DC}, which depends on the amount of neurotransmitter released per presynaptic action potential and the density of receptors on the postsynaptic membrane, are unlikely to be quickly changeable in response to a temperature change. (Even if the input current is not constant in time, its maximum or typical amplitude, of which we are taking I_{DC} as a rough estimate, would depend on these properties and not be quickly changeable.) That is, for our purposes, we will assume that both G_L and I_{DC} are essentially fixed.

With these assumptions, Fig. 7 makes it clear that values of I_{DC} in the vicinity of 3 μA are preferable to values much lower or higher in order for repetitive firing to be possible over the widest possible temperature range. For example, if I_{DC} were 4 μA and G_L 0, which gives the maximum repetitive firing frequency at 18.5 °C, a modest temperature increase of only 1.5 °C would put I_{DC} and G_L outside the region of parameter space where repetitive firing can occur. The axon would be rendered inoperable.

Assuming that I_{DC} must be around 3 μA in order for the squid giant axon to function effectively at warmer temperatures means G_L should be at a value which in general gives the highest possible f_r value at that I_{DC}. We can see from Fig. 7 that over most of the temperature range, the optimal G_L values at $I_{DC}\approx 3$ μA are clustered around 0.2 mS/cm^2. Therefore, we may expect that G_L values in the experimental range are most optimal for repetitive firing given the typical temperature variations the squid encounters. In sum, for Cl^- leak channels, biological values of G_L appear optimal for maximizing the maximum or repetitive firing frequency of the axon as determined by the Hodgkin-Huxley model.

The same is not true, however, of Na^+/K^+ leak channels, which show no such optimization at nonzero G_L values for the maximum or repetitive firing frequencies. They only appear to be superior in this regard to Cl^- channels when it comes to the relative refractory period as defined for a maximum allowed interval shift above about 150 μs: while both models evince nonzero optima for G_L, the one for Cl^- is far above the biological range of values, and the one for Na^+/K^+ is only just within it. However, the calculation of relative refractory periods is problematic for lower values of the maximum interval shift. Moreover, the relevance of the relative refractory period, which characterizes the maximum firing frequency without information loss, to a peripheral axon like the squid giant axon is not clear. Thus, we consider our results for the firing frequency associated with the relative refractory period to be much less compelling than those for the absolute and repetitive firing frequencies.

V. CONCLUSIONS

If one assumes that it is best for the squid's brain to be able to send two or more signals to its escape jet system with as little delay between them as possible, and also that the Hodgkin-Huxley model is a sufficiently accurate model of the biological squid giant axon, then the experimentally measured range of values for the squid giant axon leak conductance make far more sense for a chloride-like leak current than for one composed of separate sodium and potassium leak currents. The leak conductance appears to be optimal for the firing rate of the axon, whether it be driven by discrete input current pulses or a by constant input current, if the leak current is assumed to be chloride or some combination of ions whose overall reversal potential is approximately E_{Cl}. If the leak current is instead assumed to be composed of separate sodium and potassium currents, then no such optimization is evident, though there is weak evidence of a partial optimization for relative refractory period. It should be remembered, though, that these results are all within the context of the Hodgkin-Huxley model.

Of considerably more interest than the evolutionary neurobiology of *Loligo* is whether such an optimization of the leak conductance for firing rates exists or has taken place in mammalian central neurons. Due to the current lack of precise data on channel densities and kinetics in these much smaller and more morphologically complex cells, it is hard to address such questions in a rigorous way with modeling studies. Nevertheless, whenever such data become available, it may be fruitful to examine in detail the role of the leak conductance on firing frequencies and information rates, as it appears to be a powerful mechanism for influencing these properties despite its deceptively small magnitude.

ACKNOWLEDGMENTS

We thank J. Amato, K. Andresen, K. Belanger, W. B. Levy, J. Meyers, and K. Segall for useful discussions, as well as our referees at Physical Review E for reviewing our paper.

[1] W. B. Levy and R. A. Baxter, Neural Comput. **8**, 531 (1996).
[2] W. B. Levy and R. A. Baxter, J. Neurosci. **22**, 4746 (2002).
[3] D. H. Goldberg, A. P. Sripati, and A. G. Andreou, Neurocomputing **52-54**, 39 (2003).
[4] R. H. Adrian, Proc. R. Soc. London, Ser. B **189**, 81 (1975).
[5] A. L. Hodgkin, Proc. R. Soc. London, Ser. B **270**, 297 (1975).
[6] T. D. Sangrey, W. O. Friesen, and W. B. Levy, J. Neurophysiol. **91**, 2541 (2004).
[7] P. Crotty, T. D. Sangrey, and W. B. Levy, J. Neurophysiol. **96**, 1237 (2006).
[8] W. B. Levy, T. D. Sangrey, W. O. Friesen, and P. Crotty, J. Neurophysiol. **96**, 960 (2006).
[9] B. Hille, *Ion Channels of Excitable Membranes* (Sinauer Associates, Sunderland, MA, 2001).
[10] D. C. Chang, Biophys. J. **50**, 1095 (1986).
[11] J. R. Clay, Biophys. J. **54**, 969 (1988).
[12] B. Lu, Y. Su, S. Das, J. Liu, J. Xia, and D. Ren, Cell **129**, 371 (2007).
[13] A. L. Hodgkin and A. F. Huxley, J. Physiol. (London) **116**, 473 (1952).
[14] A. L. Hodgkin and A. F. Huxley, J. Physiol. (London) **117**, 500 (1952).
[15] C. A. Vandenberg and F. Bezanilla, Biophys. J. **60**, 1511 (1991).
[16] J. R. Clay, Prog. Biophys. Mol. Biol. **88**, 59 (2005).
[17] L. J. Gentet, G. J. Stuart, and J. D. Clements, Biophys. J. **79**, 314 (2000).
[18] M. L. Hines and N. T. Carnevale, Neural Comput. **9**, 1179 (1997).
[19] P. Crotty and W. B. Levy, Neurocomputing **69**, 1006 (2006).
[20] J. Rinzel, J. Math. Biol. **5**, 363 (1978).
[21] J. J. C. Rosenthal and F. Bezanilla, Biol. Bull. **199**, 135 (2000).
[22] P. W. Gage and J. W. Moore, Science **166**, 510 (1969).
[23] T. Preuss and W. F. Gilly, J. Exp. Biol. **203**, 559 (2000).
[24] Y. Kawai and A. Wada, J. Oceanogr. **63**, 721 (2007).